Optically active CdSe/CdS nanoplatelets exhibiting both circular dichroism and circularly polarized luminescence

Junjie Hao, Fenghuan Zhao, Qiushi Wang, Jiaying Lin, Peixian Chen, Junzi Li, Dongxiang Zhang, Meijuan Chen, Peizhao Liu, Marie-Hélène Delville, et al.

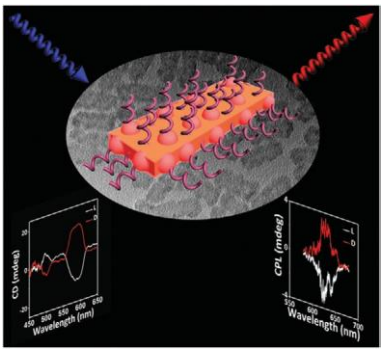

In this paper, chiroptical 2D CdSe/CdS nanoplatelets (NPLs) are prepared by ligand exchange approach, exhibiting both circular dichroism (CD) and circularly polarized luminescence (CPL). Furthermore, the CD and CPL signals are easily tuned via the design of the CdS-island structura- tion of the shell and its thickness which are controlled with the reaction time.

Optically Active CdSe/CdS Nanoplatelets Exhibiting Both Circular Dichroism and Circularly Polarized Luminescence

Junjie Hao, Fenghuan Zhao, Qiushi Wang, Jiaying Lin, Peixian Chen, Junzi Li, Dongxiang Zhang, Meijuan Chen, Peizhao Liu, Marie-Helene Delville, Tingchao He,* Jiaji Cheng,* and Yiwen Li**

Ligand-induced chirality in colloidal semiconductor nanocrystals attracts attention because of their tunable chiroptical properties. Here, the induced chirality and circularly polarized luminescence (CPL) are investigated as a function of the CdS shell growth in a range of 2D CdSe/CdS nanoplatelets (NPLs) capped with chiral ligands. Five samples of CdSe/CdS NPLs are synthesized by a one-pot approach to vary the island-like shell on a four-monolayer (4 ML) CdSe NPLs core, which effectively reduces the interfacial strain energy. The successful preparation of L-/D-Cysteine-capped CdSe/CdS NPLs with both tunable circular dichroism (CD) and CPL behaviors and a maximum anisotropic luminance factor (g_{lum}) of 5.29×10^{-4} is described. The induced chiroptical response shows a direct relationship with the formation of island-like shell in the first and second stages and shows a clear signal evolution. In the third stage with a full coating shell, the CD and CPL signals are inversely proportional to the CdS shell thickness. The island-like shell gives birth to the CPL signal, while the formation of full coating shell decreases the induced chirality. Such chiral and emissive NPLs provide an ideal platform for the rational design of semiconductor nanocrystals with chiroptical properties in areas of biomedicine, polarizers, and new generation of display devices.

1. Introduction

Induction of optical activity into inorganic semiconductor nanocrystals (NCs) is a promising way to introduce a new dimension of updates to their properties, which can be used in stereoselective synthesis,[1–3] chiral recognition,[4,5] display devices,[6,7] biosensing,[8,9] asymmetric catalysis,[10] and so forth.[11–13] Gun'ko and colleagues, for example, were the first to report the observation of a circular dichroism (CD) response induced in the excitonic transitions of CdS quantum dots (QDs) capped with chiral molecules.[14] Gener- ally, chirality in QDs can originate from a range of mechanisms including a chiral shell layer,[14–17] chiral dislocations and defects,[1,3,18] ligand-induced chirality,[19–21] and chiral assemblies.[2,22–24] Among these mechanisms, ligand exchange with chiral molecules has led to significant progress in obtaining QDs with a uniform size distribution and designing QDs surface chemistry to impart the overall chemical properties. However, circularly polarized luminescence (CPL), a counterpart of CD in terms of emission, has seldom been reported in semiconductor NCs because of the low accessibility of CPL instruments, insufficient theoretical background on this topic, and a complex experimental control that is required over the synthesis. Up to now, only the spherical and rod-shaped semiconductor NCs samples with chiral-ligand-induced CPL have been reported,[20,25–27] in which L- and D-Cysteine (Cys) play a pivotal role for the CD and CPL performances. There- fore, the regulation of these optical phenomena by feasible parameters, including CdSe/CdS QD morphologies and sizes, has been of great interest to researchers in recent years.

In semiconductors, the shape is an important parameter due to its important effects not only on the electronic states of charge carriers but also on the optical properties of the NCs.[28] For example, the density of electron and hole states changes from discrete levels for 0D (QDs), to a saw-like quasi-con- tinuum in 1D nanorods (NRs), and finally to the step-like quasi- continuum in 2D nanoplatelets (NPLs). Thanks to the excellent properties of NPLs, such as short fluorescence lifetime,[29] wide tunability of both narrow absorption and photoluminescence (PL) lines,[30–32] as well as low lasing thresholds,[33] they have recently become an emerging topic of interest. As compared with spherical QDs and NRs, NPLs have a much stronger quantum confinement in the transverse direction, and a larger surface to volume ratio, which are critical parameters for the

J. Hao, Q. Wang, J. Lin, P. Chen, D. Zhang, M. Chen, J. Cheng, Y. Li
School of Materials Science and Engineering
Hubei Univeristy
Wuhan 430062, China
E-mail: jiajicheng@hubu.edu.cn; yiwenli@hubu.edu.cn
J. Hao, F. Zhao, P. Liu, M.-H. Delville
ICMCB
CNRS, Univ Bordeaux
UMR, Pessac F-33608, France
E-mail: Marie-Helene.Delville@icmcb.cnrs.fr
J. Lin, J. Li, T. He
College of Physics and Energy
Shenzhen University
Shenzhen 518060, China
E-mail:tche@szu.edu.cn
The ORCID identification number(s) for the author(s) of this article can be found under https://doi.org/10.1002/adom.202101142.

induction of chirality. However, similar to other classes of col- loidal semiconductor NCs,[34–37] core-only NPLs suffer from poor stability owing to their large surface area that results in lower PL quantum yield (PL-QY),[31] however a necessary con- dition for CPL signals. Up to now, to enhance the PL-QY and stability of NPLs, core/crown (laterally grown shell)[31,38,39] and core/shell (vertically grown shell)[31,32,40] architectures have been synthesized and studied intensively. The PL-QY can be signifi- cantly increased in the core/crown NPLs, thanks to the passi- vation of the trap sites originating from the sidewall of core- only NPLs.[31] However, since the CdS-crown layer is grown only in the lateral direction, they still suffer from serious sta- bility issues. The PL-QY can be greatly quenched in the core/ crown NPLs after a common chiral ligands exchange process,[41] because of the lack of proper passivation on their larger lateral surfaces. Also, with the coating of a flat CdS shell, the optical properties of the CdSe/CdS core/shell NPLs have been shown to be enhanced with respect to the core-only NPLs. This shell build-up is carried out by the colloidal atomic-layer-deposi- tion (c-ALD) technique. This layer-by-layer (LBL) method can improve the stability of NPLs in aqueous phase, while the intense CD signal almost completely disappears after coating with a very thin flat CdS shell and no CPL was reported.[21] The LBL processes are very useful when a fine control of the shell composition is needed, however when thick shells are required, the application of an LBL protocol is time-consuming and the NCs need to be carefully washed in between each layer to pre- vent secondary nucleation. Recently, Dubertret et al.[30,32] pre- sented a simple continuous shell growth in a one-pot approach performed at room temperature, in which the exciton was also confined within the core of the heterostructure and away from the lateral surface traps and possible dangling bonds. With the formation of polytypism shell layers, a significant amount of spectral red-shift is observed in the absorption and emis- sion spectra depending on the thickness and composition of the shell layers. Therefore, the island-like shell coincided with chiral anisotropy, and a higher level of PL-QY (up to 80%) could be achieved, with a high potential to release CPL signals.

Herein, we report a comprehensive investigation on the combined effects of chiral ligand exchange on both induced CD and CPL signals, by varying the thickness of the island-like shell, leading to an optimal NPLs nanostructure with both a strong excitonic chiral emission and a well-expressed chiral ligand- induced CD activity. In particular, the effects of the purification process and reaction time are first investigated to obtain high quality (high yields with size precision, PL-QY, monodisperse and low impurity) chiral CdSe/CdS NPLs. It is followed by a systematic study of the CD and CPL signals with the CdS shell growth, to provide not only deep insights into how experimental parameters can impact the formation of CdSe/CdS island-like nanostructures, but also information about how the shape vari- ations and shell thickness can affect ligand-induced chirality in terms of CD and CPL behaviors, respectively.

2. Results and Discussion

To activate both CD and CPL responses, a one-pot approach is used to form the core/shell structures, as indicated in the Experimental Section. We synthesized them using the same process as described in the literature with little modifications to further study the formation process of the island-like shell.[30,32] The four-monolayer (4 ML) zinc blende (ZB) CdSe NPLs cores were prepared based on the reaction between cadmium myristate and Se powder in 1-octadecene at 240 °C, protected by an addi- tional layer of Cd atoms in oleic acid.

The CdSe/CdS core/shell NPLs were synthesized in one-pot by mixing CdSe NPLs cores, $Cd(OA)_2$, and the thioacetamide (TAA) at room temperature. When TAA is introduced in the NPLs solution, the PL emission of CdSe NPLs is quenched and the solution turns from yellow to orange in 10 min.[31] With the addition of the Cd^{2+} precursor, the island-shaped NPLs are formed and their luminescence gradually increases, the QY can be maintained at more than 40%. During the CdS shell growth process on the initial CdSe NPLs, there was also some secondary nucleation of CdS NCs. The removal of these CdS NCs from secondary nucleation is a key factor for high CD and CPL chiral activities, which will be described in the following. As reported in the literature, when the lateral size of an NPL (length x width) is less than 100 nm^2, the CD signal increases dramatically as the size decreases, however, the g-factor or optical activity changes very little for values ≥ 100 nm^2.[21] In the one- pot shell growth process, (Table S1, Supporting Information), the lateral size significantly increases with the shell growth. Then, in order to reduce the impact of size changes on the chiral signal, we chose S0 with a size ≥ 117 nm^2 and an emission at 515 nm as the CdSe core NPLs. The full widths at half maximum (FWHM) are 14 and 9 nm for light and heavy hole bands, respectively (Figure S1, Supporting Information). The extremely narrow peaks are attributed to the strong quantum confinement effect in ultrathin 2D nanostructures. The observed absorption peaks indicate that the NPLs thickness herein is around 4 MLs based on previous studies.[21,31,32,41] These obtained 4 MLs CdSe NPLs core with lateral dimensions ≥ 5.3 nm ≥ 21.9 nm and 1.4 nm thickness (Figure S2, Supporting Information), have a ZB struc- ture, and their two largest facets end with a cadmium-rich plane are passivated by carboxylate ligands.[41,42]

The L/D-Cysteine (L/D-Cys) was chosen as the chirality induction ligands; the absorption spectrum of L-Cys NPLs in Figure S3, Supporting Information, shows a significant red shift of Cysteine-stabilized CdSe NPLs compared to the oleate-capped ones. This strong shift may be due to the exciton extension into the two additional monolayers of the thiolate functions once the ligand exchange is complete, the exciton extension is originally limited to the CdSe NPLs. Additionally, the first two excitonic transitions, involving light hole (e-lh) and heavy hole (e-hh), are not as sharp as in the case of CdSe core-only NPLs. This broad- ening of the excitonic transitions may be due to ligand density variations between NPLs.[32] In order to scrutinize the NPLs chiroptical properties, we investigated parameters such as the purity of the samples and the influence of purification as well as the different stages of the CdS shell growth which might signifi- cantly affect the CD and CPL signals.

2.1. Effect of Purification

First, we studied the effect of purification. Indeed, as shown in Figure S2, Supporting Information, for the CdSe NPLs core,

there are plenty of spherical particles formed during the NPLs synthesis process. Since the g-factor is inversely proportional to the UV absorption and the purification process can effectively remove byproducts, the latter becomes critical for the accuracy of chiral signals. As an example, Figure S4, Supporting Infor- mation, compares the two data sets for L/D-CdSe particles with and without purification, confirming that purification is essen- tial for chirality, with a g-factor for the purified sample three times higher than the raw samples. This is due to the presence of these spheres which have weaker ligand-induced CD signals (≈10^{-5}) and absorbance at different wavelengths.[19]

In addition, our results also clearly confirm that the purifica- tion process is also crucial during shell growth. As shown in the references,[30,32] even if the one-pot preparation easily pro- duces CdS self-nucleation by-products, pure nanosheets can nevertheless be obtained through a simple purification process, and in our case, this purity can be easily checked thanks to the CPL sensitivity. As shown in the TEM images in Figure S5(a-d), Supporting Information, the island-like shell NPLs were puri- fied and isolated from the secondary nucleation of CdS NCs by precipitation with a few drops of ethanol. Although self-nuclea- tion has little effect on the fluorescence spectrum (CdS has no visible light emission) (Figure S5f, Supporting Information), it has a great effect on the absorption one (Figure S5e, Sup- porting Information). By pre-removing secondary nucleation of CdS NPs due to their size difference, the CD signals of the nanosheets can be better reflected. In comparison, during the c-ALD method, more purification processes are needed to get pure core/shell NPLs.[31,32] Each time before adding the Cd^{2+} or S^{2-} precursors, the mixture solution needs to be purified to remove the excess precursor and prevent the secondary nuclea- tion. When thick shells are needed, the application of a layer-by layer protocol becomes too time-consuming. Additionally, these washing steps also break the remaining S or Cd bonds on the NPLs surface and produce reactive sites. It is more difficult to get pure NPLs by c-ALD method, which may affect the CD signals.

2.2. Effect of Reaction Time

Island-like shell CdSe/CdS NPLs synthesis[32] was explored over reaction times from 0 to 180 min (Tables S2 and S3, Sup- porting Information) and analyzed by both PL emission and transmission electron microscopy (Figure S6, Supporting Infor- mation, and **Figure 1**). As shown in Figure S6a, Supporting Information, the cadmium precursor was added over three hours and the PL emission of the resulting island-like NPLs in the organic phase gradually red-shifted from 515 to 638 nm, and the FWHM increased from 12 to 23 nm under the excita- tion wavelength of 450 nm. A more accurate study of this emis- sion wavelength variation with the reaction time reveals an asymptotic behavior (Figure S6b, Supporting Information) with a large red-shift at the beginning which can be explained by the fact that the 2D confinement of the exciton, initially limited to CdSe, extends to the additional monolayers of the NPLs. The FWHM displays a strong increase after the first 10–30 min to reach a constant value (23 nm) as the shell thickness increases, indicating that the size distribution of the island-like NPLs improves during the shelling procedure. Although a significant broadening of the emission is observed in the island-like shell CdSe/CdS NPLs compared with the CdSe core NPLs, it is still narrower than that of other classes of colloidal semiconductor NCs including QDs and NRs.[34,37] This behavior is completely different from the step-like quasi-continuum NPLs obtained by c-ALD. For instance, although the c-ALD method offers great advantages including the formation of a smooth CdS shell layer with atomically precise control of the shell thickness, the emission jumped to 586, 630, and 645 nm without continuous evolution, which is consistent with the growth of one, two, and three CdS monolayers.[31] Compared with the stepwise shell growth process, the island-shell one allows a finer more pro- gressive tuning, which promotes a precise regulation of the nanoparticles morphology and the chiral signal once the chiral ligand is added.

The PL-QY of NPLs varied from 5 to 40% across samples S1–S5 (Table S2, Supporting Information), with an initial increase up to S4 and then a slight reduction as the shell growth con- tinued. This further minor decrease in QY may be due to the crystal defects into the shell via lattice mismatch between the CdSe core and CdS shell or the effects of disordered structures present in the island-like shell,[43] which increase as the shell growth process takes place.[44] Furthermore, for the core/island- shell NPLs, the emission FWHM remained narrow while the QY steadily increased up to maximal values of ≈ 40% (for reac- tion times between 60 and 120 min). However, although the island growth is beneficial in releasing the misfit strain energy, the overall thickness of the CdS shell still increases during the island's growth, producing additional interfacial defects, which lead to further quenching of the emission intensity for S5.

This island-like shell structuration during the different steps of the CdS growth is visible in Figure 1, where most of the "core/shell" NPLs are deposited on their highest surface on the TEM grid Figure 1b–f and only a few of them still stand on their edge as opposed to the core NPLs behavior in Figure 1a. The reaction time is started after the source of cadmium is added. In fact, the strain energy induced by the lattice mis- match between the CdSe core and CdS shell accumulates and above a critical CdS thickness, a 3D island growth is favored to relieve the misfit strain, leading to the formation of islands.[45]

Despite the lattice mismatch between CdSe and CdS being relatively small (4–6 %),[46] and the large specific surface area of the NPLs that makes them bend,[29] it is still more likely to generate defects during the shell growth process than 0D QDs or 1D NRs. Fortunately, the structuration in islands can effec- tively reduce the strain energy caused by lattice dislocation. These TEM images show that the reaction time effectively plays a critical role on both the shell lateral size and shape with a progressive decrease of the number of bumps (islands) as time evolves and as they grow (compare Figure 1b,1f, see Table S1, Supporting Information) confirming data obtained by PL anal- ysis (Figure S6, Supporting Information).

Examining both Figure 1 and Figure S7, Supporting Infor- mation, we can confirm their island-like CdS shell growth around the CdSe NPLs. It is already effective in 10 min (thanks to the edges we can detect up to four islands along the longest NPLs dimension (yellow arrows, Figure S7b, Supporting Infor- mation), when the number of islands increases even if that of

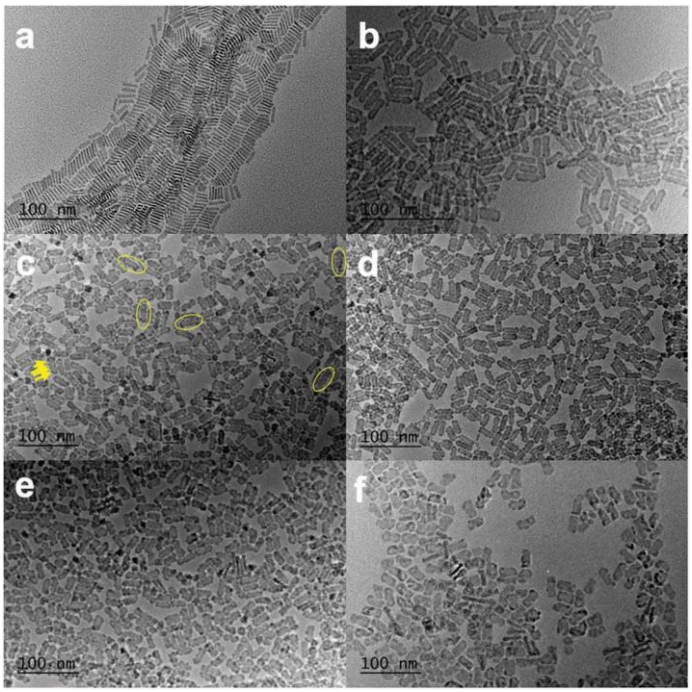

Figure 1. The growth evolution of island-like CdS shell modified NPLs. a) S0-CdSe NPLs, b) S1-10 min, c) S2-30 min, d) S3-60 min, e) S4-120 min, f) S5-180 min. The scale bar on each image is 100 nm. Yellow arrows indicate bumps on the NPL edge, ovals show NPLs with up to four bumps on the longest dimension.

islands on the edge seems to be the same at least in Figure 1c (yellow arrows and yellow ovals) and Figure S7c, Supporting Information, the spacing in between them gets less and less regular (Figure 1c,d, Figure S7c,d, Supporting Information, orange and white arrows). Indeed, the surface of the CdSe core NPLs still has free sites where the CdS shell can mainly grow in an island-like shape before coalescence, explaining why the lateral size does not increase in this stage. Finally, as the growth proceeds for more than 120 min (S4,S5, Figure 1e,f and Figure S7e,f, Supporting Information), the surface of the CdSe core NPLs is completely covered, the islands-like CdS shell can only go on growing on itself which leads to a decrease of the number of islands.

The absorption and emission spectra are similar to those of the core/shell NPLs by c-ALD.[31,32] Then, whether the thickness of the NPL is gradually increased with the reaction time from 1.4 nm for the core to 6.0 nm or made by an LBL process, does not matter for the synthesis of these nanoobjects, and a one- pot process is much preferable. The thicker CdS shell is also demonstrated by the strong absorption increase below 510 nm (Figure S8, Supporting Information), a value close to the CdS bandgap. The anisotropic structure of the NPLs CdS shell shown at different steps of the shell growth by TEM images along (Figure 1b–f, Figure S7(b-f), Supporting Information) is the key factor to get an excellent chiral signal.

2.3. Shell Growth Dependence of CD and CPL Signals

To develop a better understanding of the reasons for these excellent chiral signals, such as the birth of the CPL signals and the enhancement of the CD signals, we studied the variation of the chiral properties with the growth of the island-like shell from controlled island-like shell to real core/shell NPLs. By con- trolling this island-like shell growth process, we aim to achieve high CPL signal-coupling while maintaining a high CD signal.

The ligand-induced chirality of NPLs was obtained by a ligand exchange, which also transferred the NPLs from the organic phase to the aqueous solution, and was followed by a subsequent storage in excess of aqueous Cysteine solution over- night prior to measurements. The ligand exchange of the NPLs samples was performed for both L- and D-Cysteine ligands, and the optical properties of the samples were examined using CD and CPL. The absorption and induced CD response of a series

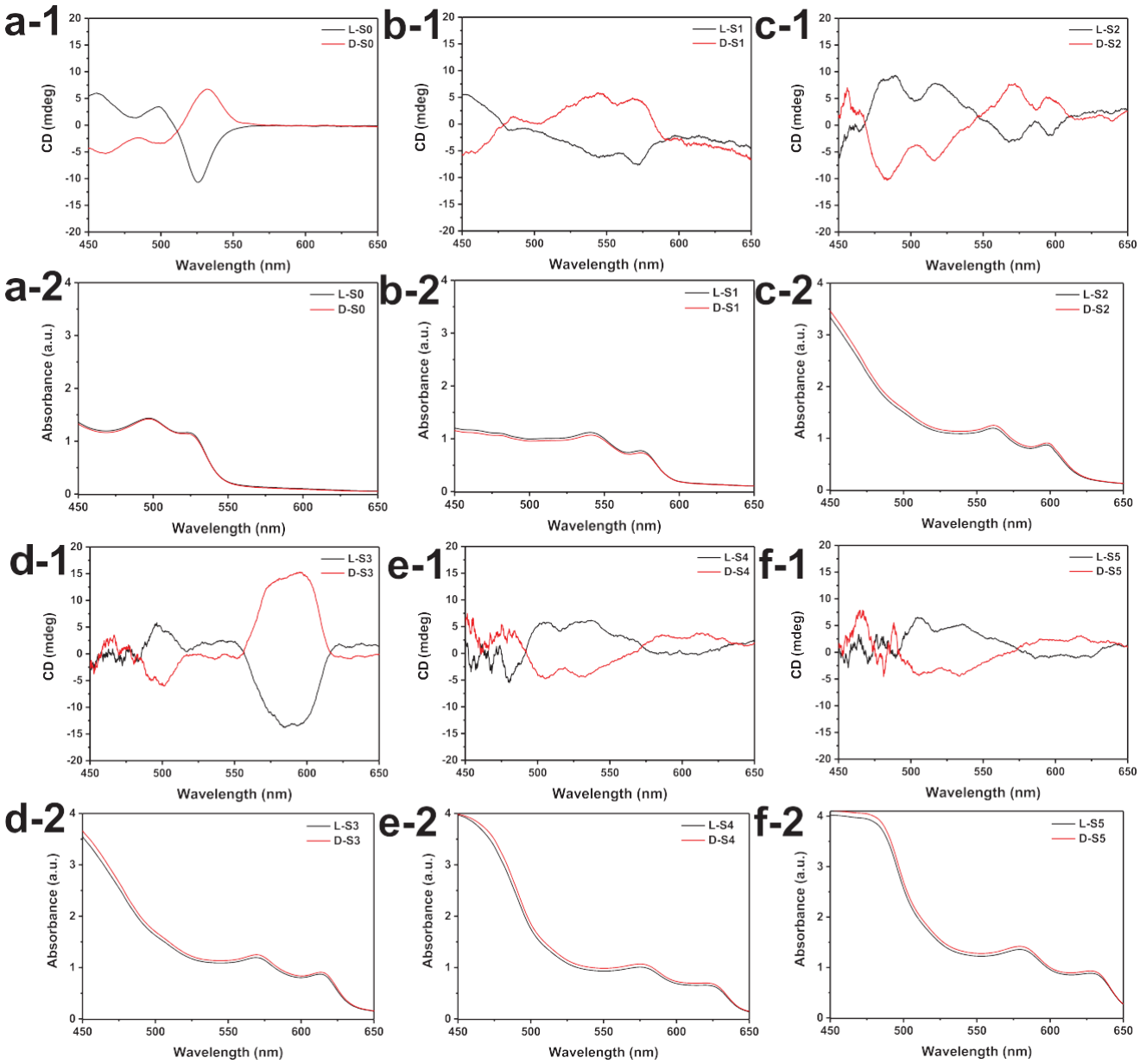

Figure 2. The CD and absorption spectra between 450 to 650 nm of a series of a) CdSe NPLs core and b–f) island-like CdSe/CdS core/shell NPLs (samples S1 to S5).

of CdSe NPLs core and island-like CdSe/CdS core/shell NPLs (S0 to S5) as a function of the growing shell between 450 to 650 nm are presented in **Figure 2**, Figure S9 and Table S4, Sup- porting Information.

The samples were measured at similar optical densities (at the first band edge peak position, ⍰1.0) to make sure the CD strength did not depend on the relative absorption. The CD peaks correspond to the NPLs excitonic bands, following the same redshift with the increase of the shell thickness. In addition, unlike the literature reports,[21] the "Cotton effect" gradually appears with the island-like shell growth, though at present the precise mechanism of this coupling is unknown. The dependence of the g-factor value on the reaction time (Figure S10, Tables S4 and S5, Supporting Information) is quite complicated; first, the g-factor of island-like NPLs gradu- ally increases with the shell growth, goes through a maximum value (S3, 60 min) before decreasing again in a significant way. To explain the mechanism for this induced chirality varia- tion, we propose a three-step growth mechanism for the island-like shell NPLs growth process as illustrated in **Figure 3**.

In the first stage, discrete CdS islands shell begins to appear all over the CdSe core NPLs (0–30 min). With the formation of these discrete island CdS shells all over the periphery of the CdSe-core NPLs, the PL-QY can be enhanced as the trap sites are gradually passivated. They also enhance the geometry ani- sotropy of the surface and provide the possibility for the chiral

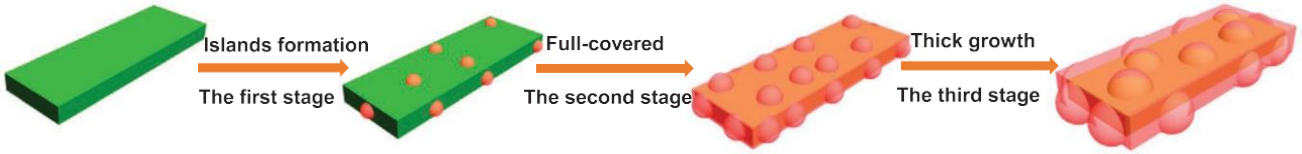

Figure 3. Growth mechanism of island-like shell CdSe/CdS NPLs. The one-pot growth process is divided into three stages: In the first stage, the island- like shell forms on the surface of CdSe NPLs. And then, in the second stage, a thin shell forms in between all the islands. Last, this thicker overall shell further grows with time.

ligands to still come into close contact with CdSe-core NPLs or even directly,[19] which may be the key factor for the excel- lent anisotropic properties. It has indeed been shown that the interfacial strain energy can be reduced as the CdS shell is tuned from flat to island-like structure,[45] while crystal defects inducing epitaxial growth are decreased. The strain energy gen- erated by the lattice mismatch between the two materials accu- mulates and above a critical thickness, a 3D island growth is favored to relieve the misfit strain, leading to better stability. As a result, in this stage, a CPL signal is also generated along with the enhanced CD signal while maintaining the initial CD signal (see below).

In the second stage, the density of islands increases and they begin to form an island-like shell with both enhanced CPL and CD signals (30–60 min). In the final stage, the surface of the nanosheet is completely covered, and, further growth of the CdS shell leads to some coalescence of the islands and a gradual quenching of the emission intensity accompanied by a gradual decrease of the induced chirality. In this process, although the polytypic island growth is beneficial to release the misfit strain energy and improve the anisotropic properties, at some point when it reaches completion, it produces a decrease in chiral conduction. This result is in excellent agreement with previous results mentioning the CD signals decrease with the shell thickness and subsequent distance increase between the hole present in the CdSe core and the coordinated chiral ligands on the surface of the QD.[19,21] Therefore, we have high- lighted the critical importance of controlling the anisotropic morphology during shell growth to drive the performance gain of CPLs. Besides its fundamental interest, we believe that this study could help identify potential applications for core/shell NPLs.

We corroborated this schematic analysis with the study of the respective sizes of these different stages by TEM (Table S1 and Figures S11 and S12, Supporting Information), on at least 100 NCs. Figure S11, Supporting Information, illustrates the variation of the NPLs lateral size as well as that of the g-factor (Figure S11a, Supporting Information) and the quantum yield (QY) (Figure S11b, Supporting Information). The quick increase in less than 30 min corresponds to the formation of discrete, non-uniform in size, first CdS islands (stage 1). This lateral size remained the same during the second stage from 30 to 90 min, while the CdSe core NPLs coverage density with island-like CdS shell increased, that is, while the CdS also begins to fill in the spaces in between the islands. As long as the surface of CdSe core NPLs still exhibits bare surface areas, the CdS shell mainly goes on growing on these CdSe surfaces, which does not modify the lateral size (stage 2). Finally, beyond 120 min, the surface of CdSe core NPLs is completely covered, the island-like CdS shell can only go on growing on the surface of the existing CdS shell, which again leads to the significant increase of lateral size (stage 3).

In the first and second stages, due to the formation of the island-like structures, there are still many exposed CdSe areas on the surface of the CdSe core NPLs, and the ligand can directly link the core or be in close contact with it. The high CD signals can be maintained. At the same time, thanks to the island-like structure, the anisotropy of the NPLs can fur- ther improve the chiral signals. Note that g begins to increase once the lateral size does not change anymore and has reached a high anisotropy, the highest one being obtained for 60 min reaction time. Then at the end of the second stage and in the third one, the CdSe core NPLs are completely encapsulated after more shell precursors have reacted. The resulting chiral response of the sample is thus strongly reduced due to the increased distance between the hole present in the CdSe NPLs core and the coordinated Cys- chiral ligands on the surface of the NPLs, explaining why the CD signals of the NPLs is greatly decreased after 2 h of shell growth (Figure S11a, Supporting Information).[21] This result was unexpected because the initial anticipation was that the strong CD signal observed in the CdSe core NPLs would almost completely disappear in the core/ shell NPLs.[21] Instead, it was determined that the presence of an island-like shell increased the measured CD response. The second intriguing feature arises from the dramatic difference between the induced CD response in core/shell and core/crown CdSe/CdS NPLs. The washing out of the CD features upon an increase of the spatial separation between the CdSe core and the chiral ligands with the growth of a single CdS ML is more pronounced in NPLs, likely due to the smaller effective Bohr radius and the structural anisotropy.

We also studied the CD response variation of the CdS shells (between 350 to 500 nm), as shown in Figures S13–S15 and Tables S6 and S7, Supporting Information, and mainly induced by the anisotropy of the island-like CdS shell. In the first stage, the anisotropy increased with the island-like shell formation. While in the second stage, it decreased due to the higher den- sity of CdS shell. Finally, in the third stage, the growth of the CdS shell layer further reduces the anisotropy. The activation of chiral emission from these chiral island-like shell NPLs can therefore be rationally envisioned after the successful observa- tion of enhanced induced chirality in the CD measurements.

The corresponding CPL spectra of these samples are dis- played in **Figure 4** for both enantiomers. As expected, oppo- site line shapes are observed for the CPL spectra within the PL-active region. The CPL spectrum reflects the intensity dif- ference of the emission; thus, it is always accompanied by the emission spectrum.[47] Upon the CdS shell growth on CdSe

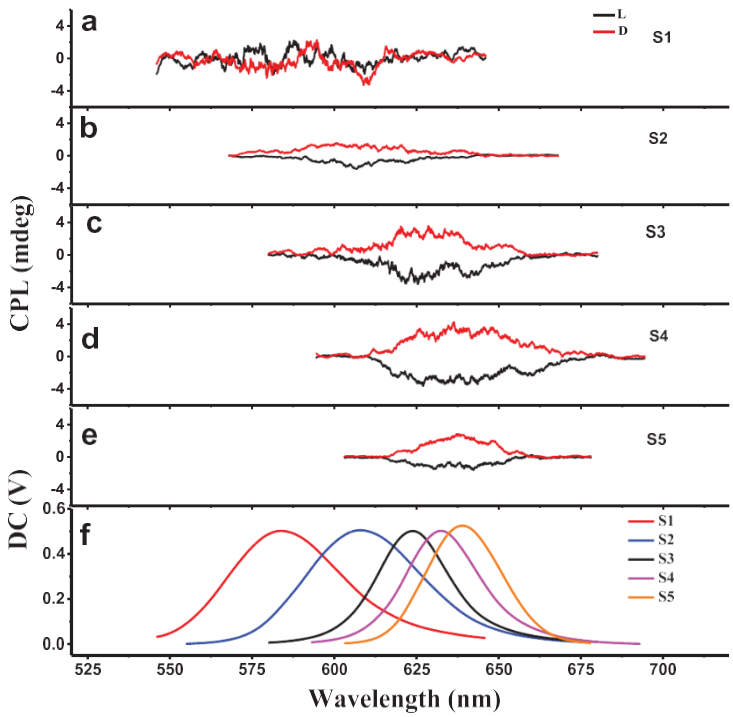

Figure 4. a–e) CPL spectra of a series of island-like CdSe/CdS core/shell NPLs with different growth stages S1-S5 after Cysteine ligand exchange treatments. f) Corresponding DC voltage spectra of L-Cys capped CdSe/CdS core/shell NPLs.

NCs, a consequence of the exciton delocalization in the CdS shell region, a continuous redshift of the first exciton absorp- tion peak and band-edge PL peak is observed (Figure S6, Sup- porting Information), which has also been reported by Peng's group.[46,48] Therefore, as the fluorescence spectrum moves to a longer wavelength, the redshift of the CPL active region with the island-like shell growth is also effective (Figure 4).

The PL and PL-QY are known to be highly important optical properties of the NPLs, especially in relation to the CPL activity. Similar to other classes of colloidal semiconductor NCs,[37] core- only NPLs have suffered from poor stability due to their large surface area that results in a lower PL-QY.[31] The stability issues and low PL-QYs prevent CPL signals from being generated. A common consequence of ligand exchanges is then a strong reduction in NCs PL, due to the large specific surface area; it is especially serious for NPLs. In the core/crown system,[21,31] due to the formation of surface trap states in the large bare lateral area of CdSe exposed on both sides, after ligand exchange, the fluorescence is almost completely quenched (≈ 5%), unable to generate CPL signal. In the c-ALD method, although the high QY can be maintained, due to the thick shell of CdS overall coating, up to now, there was no CPL signal reported.

In the one-pot reaction process, we propose, as shown in Table S3, Supporting Information, the PL-QY is maintained to more than 20% and can reach up to 25% after the ligands exchange from the organic phase to the aqueous phase. This is due to this island-like shell effect of CdS in the CdSe/CdS NPLs which can effectively reduce the stress caused by lattice dislocation.[45] The high QY can then be maintained as long the coverage is not total. Indeed, in the third stage, the island shape shell gradually forms a complete overcoating shell, which increases the lattice misalignment resulting in a small decrease of PL-QY.

The three-stage growth process is also confirmed by the CPL tests. As shown in Figure 4. First, due to the partial expo- sure of CdSe in the initial stage, after the ligand exchange, more defects are generated, and the fluorescence quenching is severe, no CPL signal can be obtained. In the second stage, since more and more CdSe surface is protected, a high QY can be maintained after the ligand exchange; this lays the founda- tion for CPL generation. At the same time, due to the island structure, the distance between the ligand and the NPL core is small, which is beneficial for the generation of emission chi- rality. While in the final stage, the thickness shell can effectively

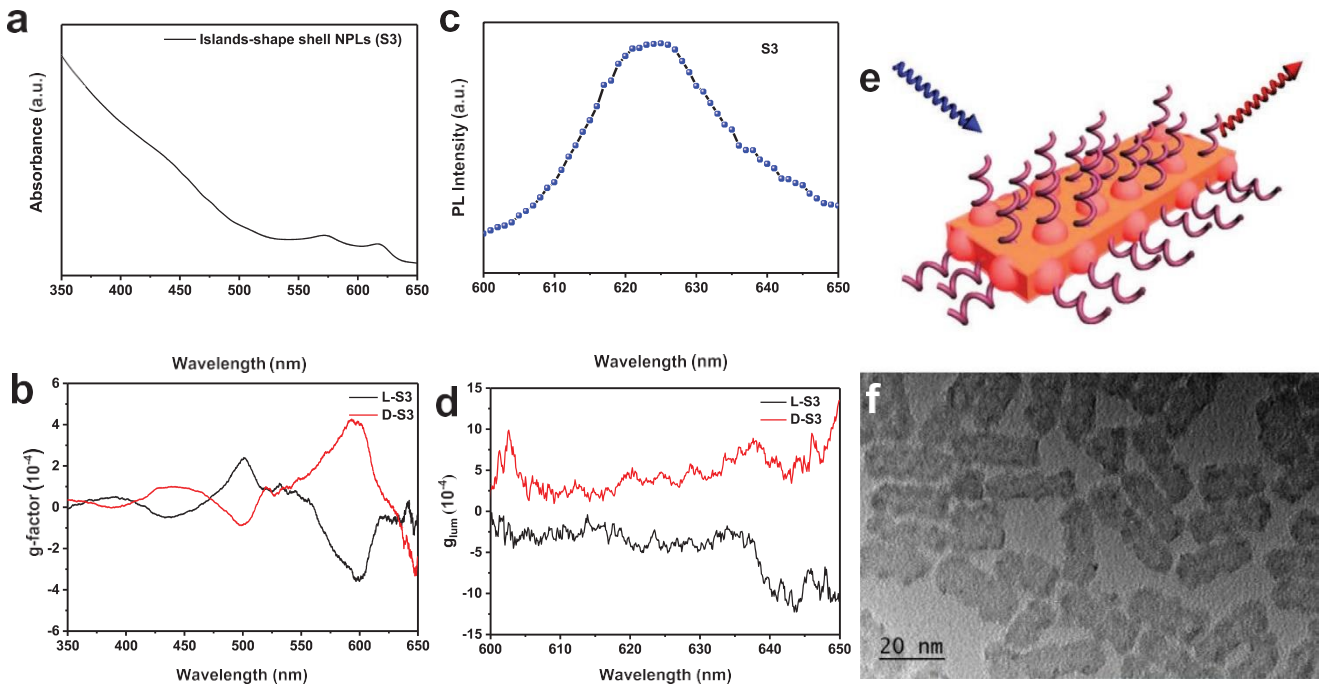

Figure 5. Island-like CdS shell modified NPLs (S3) exhibiting both CD and CPL signals. a,b) Their UV absorption and CD g-factor; c,d) Their PL emis- sion and CPL g_{lum}; e) The schematic diagram of NPLs chiral signals; f) The TEM images of island-like CdS shell modified NPLs. The scale bar is 20 nm. The CD and CPL originate from interactions with chiral cysteine molecules as depicted in (e).

decrease the ligand-induced chirality, which further decreases the CPL signals. Additionally, as in reference,[31] a decrease of the PL-QY is observed when increasing the CdS-shell thick- ness and attributed to our shell deposition method, which was performed at room temperature under ambient atmosphere, resulting in the formation of defect sites. Coupling with the decrease of anisotropy, the CPL signals will die.

Additionally, although the exact mechanism for the induc- tion of CPL still needs to be determined, the chiral interactions between the Cysteine molecules and the NPLs are asserted to be the key parameter in producing CPL, similar to their role in producing the CD response. In our experiments, the S3 was the optimal core-shell NPLs growth stage. This island-like shell CdSe/CdS NPLs achieved an excellent anisotropy, with a maximum CD g-factor maintained at 5.43 × 10^{-4}. Addition- ally, the CPL signal was initiated along with the enhanced CD signal, which has a maximum anisotropic luminance factor (g_{lum}) of 5.29 × 10^{-4}. This is the first report about CPL signals in ligand-induced chiral NPLs. All the related characterizations are shown in **Figure 5**. Because of the formation of an island- like CdS shell using a continuous shell growth in a one-pot approach, chiral CdSe/CdS NPLs show, for the first time, con-comitant strong CD and CPL responses, behavior which is very different from that of normal flat core/shell NPLs.[21]

3. Conclusion

In summary, we reported here one of the first chiral ligand-induced CPL signal in 2D colloidal semiconductor CdSe/CdS NPLs. Their CD and CPL activities were found to be sensitive to not only their surrounding chiral medium but also to their intrinsic geometrical properties. By controlling the shell growth ate, three different shell growth stages can be envisioned, from a discrete island-shaped shell formation, to an island-like shell with a higher density of islands, and eventually a com- pletely covered shell formation. Accordingly, the ligand-induced CPL activity is witnessed from null to intense and eventually becomes inactive. Moreover, we demonstrate that tuning aniso- tropic island-like shell in terms of shape and thickness can pro- vide a critical guideline for the fabrication of 2D semiconductor quantum wells with induced chiroptical activity, which provides a better understanding of the origin of ligand-induced chirop- tical effects in semiconductor nanoparticles and may potentially aid in the technological development of chiral synthesis and recognition, optical devices, and multifunctional nanomaterial design.

4. Experimental Section

Chemicals: Cadmium nitrate tetrahydrate ($Cd(NO_3)_2$ $4H_2O$, 99.997%), cadmium acetate dihydrate ($Cd(Ac)_2$ $2H_2O$, 98.0%), Cadmium oxide (CdO, 99.99%), oleic acid (OA, 90%), TAA (≥99.0%), octyl amine (99%), and tetramethyl ammonium hydroxide pentahydrate (TMAH, ≥97%) were purchased from Sigma-Aldrich. L-Cysteine hydrochloride monohydrate (99%), D-Cysteine hydrochloride monohydrate (98%), and selenium powder (Se, ≥99.999%) were purchased from Aladdin Industrial Co., Ltd. (Shanghai, China). 1-octadecene (ODE, 90%) and sodium myristate (98%) were purchased from J & K Chemical Reagent Company, China. Pure water was purchased from Hangzhou Wahaha Group Co., Ltd, China. All chemicals were used as received without further purification.

Preparation of Cadmium Myristate Precursor: Cadmium myristate was prepared according to the recipe given in the literature.[31] For a typical synthesis, 1.23 g of $Cd(NO_3)_2$ $4H_2O$ was dissolved in 40 mL of methanol and 3.13 g of sodium myristate was dissolved in 200 mL of methanol. After complete dissolution of $Cd(NO_3)_2$ $4H_2O$ and sodium

myristate powders, solutions were mixed and stirred vigorously for around 1 h. Then, the cadmium myristate ($Cd(myristate)_2$) powders were precipitated by centrifugation and re-dispersed in methanol. The washing step with methanol was performed at least three times to remove any unreacted and/or excess precursors. After successive washing steps, the precipitated part was completely dried under vacuum overnight.

Synthesis of the CdSe Core NPLs: CdSe NPLs having 4 MLs were prepared according to the procedure described in the literature with little modifications.[31] For a typical synthesis, 0.17 g (0.3 mmol) of $Cd(myristate)_2$, 0.012 g (0.15 mmol) of Se, and 15 mL of ODE were introduced into a three-neck flask. The solution was degassed at 70 °C for an hour and 100 °C for 10 min under vacuum. After degassing step, the solution was heated to 240 °C under argon atmosphere. 0.055 g (0.2 mmol, in 2 mL degassed ODE) of $Cd(Ac)_2\ 2H_2O$ was swiftly added to the reaction solution. After 10 min growth at 240 °C, 1 mL of OA was injected to further protect the NPLs, and the temperature of the solution was decreased to room temperature. By changing the cadmium precursor injection temperature and the growth time, different shapes and sizes of CdSe core NPLs can be obtained.

The Purification Process for CdSe NPLs: The resulting 4 ML CdSe NPLs were separated from other reaction products with successive purification steps. First, the resulting mixture was centrifuged at 14 500 rpm for 10 min, and the supernatant was removed from the centrifuge tube. The precipitate was dried under nitrogen, re-dispersed in hexane, and centrifuged again at 4500 rpm for 5 min. In the second step, the supernatant was separated into another centrifuge tube, and 30% ethanol was added into the supernatant solution. In the last step, after the turbid solution was centrifuged at 4500 rpm for 5 min, the precipitate was dissolved in hexane and filtered with a 0.20 μm filter.

Preparation of the $Cd(OA)_2$ Precursor Solution: $Cd(OA)_2$ were prepared by the same method in the literature.[46] The cadmium injection solution (0.2 m) was prepared by dissolving CdO (4 mmol) in oleic acid (16 mmol) and ODE (15 mL) at 250 °C under argon atmosphere. After the clear solution was obtained, the Cd injection solution was allowed to cool to about 60 °C. For each injection, the $Cd(OA)_2$ solution was diluted with the same volume of octylamine and was taken with a syringe using a standard air-free procedure.

Synthesis of the CdSe/CdS Core/Shell NPL: CdSe/CdS core/shell NPLs were prepared according to the procedure described in the literature with little modifications.[32] For a typical synthesis, 400 μL of the as-synthetized NPLs in hexane was diluted in 4 mL chloroform. 20 mg of TAA and 200 μL of octylamine were added to the flask and the mixture was sonicated until the complete dissolution of the TAA. 200 μL of a 0.1 m $Cd(OA)_2$ solution in ODE and octylamine mixture solution was then added to the reaction mixture. The reaction was allowed to proceed at different times at room temperature (from 10 min to 3 h). At various time intervals, aliquots with a needle-tip amount of the reaction mixture were removed and diluted by chloroform for further purification. The reaction rate can be controlled by changing the concentration of TAA, octylamine, and $Cd(OA)_2$.

The Purification Process for CdSe/CdS NPLs: In the CdS shell growth process on the initial CdSe NPLs, there was also some secondary nucleation of CdS NCs. After the synthesis, the CdSe/CdS core/shell NPLs can be purified from the secondary nucleation by precipitation with a few drops of ethanol and suspended in $CHCl_3$.

Ligand Exchange of the NPLs with Chiral Cysteine Molecules: The purification process in oil phase was essential for reliable chiral analysis. The spherical CdSe NCs sub-product in the core preparation process and the self-nucleation of CdS NCs in the shell preparation process did significantly affect the reproducibility of the chiral test. The L- and D-Cys ligand exchange was carried out using a previously reported method.[20,21,41]

Preparation of the L-/D-Cys Solution: D- or L-Cys hydrochloride monohydrate (0.2 m) was dissolved in DI water, and then the pH of the solution was adjusted to 12 by TMAH to form the Cysteine solution.

Ligand Exchange of the CdSe NPLs: 2 mL hexane solution containing CdSe NPLs was mixed with 2 mL of Cysteine solution. The mixture was stirred at room temperature for more than 48 h (although the NPs can transfer to the water phase in several hours, enough time incubation was crucial). The reaction mixture was left to stand for 1 h to allow the phases to separate. The bottom aqueous layer was extracted with a syringe, and the Cys-CdSe NPLs were purified by precipitation with ethanol/DI water (4:1, two times). The purified Cys-NPLs were re-dispersed in DI H_2O and stored at room temperature in the dark.

Ligand Exchange of the CdSe/CdS NPLs: 2 mL $CHCl_3$ solution containing CdSe/CdS NPLs was mixed with 2 mL of Cysteine solution. The mixture was stirred at room temperature for more than 48 h (although the NPs can transfer to the water phase in several hours, enough time incubation was crucial). The reaction mixture was left to stand for 1 h to allow the phases to separate. The top aqueous layer was collected with a syringe, and the Cys-CdSe/CdS NPLs were purified by precipitation with ethanol/DI water (4:1, two times). The purified Cys- NPLs were re-dispersed in DI H_2O and stored at room temperature in the dark.

The CdSe/CdS NPLs can be dispersed in $CHCl_3$, but were difficult to disperse in hexane or toluene.

Structural and Optical Characterization: The TEM pictures were taken using an FEI Tecnai G2 F30 microscope (300 KV) and JEOL JEM1400 Plus microscope (120 KV). The UV/vis absorption measurements were performed using a SHIMADZU UV-3600 UV–vis-NIR spectrophotometer and a TU-1901 double-beam UV/vis spectrophotometer (Beijing Purkine General Instrument Co. Ltd., China), and the PL spectra were recorded on a fluoroSENS spectrophotometer (Gilden Photonics). The absolute PL QYs of the QDs solutions were measured using an Ocean Optics FOIS-1 integrating sphere coupled with a QE65 Pro spectrometer.

CD Measurements: The measurements were conducted on a JASCO J-1500 CD spectrometer at a scan rate of 20 nm min^{-1}. All CD experiments were carried out in Milli-Q water with a quartz cuvette (0.1 cm path length, Hellma). In designing chiral nanoparticles for application, the anisotropy or g-factor was a key parameter to determine the optical activity due to its ready availability by comparing CD spectrum with the absorption spectrum. The equation is as follows: $g = \theta / 3.298 \times 10^4 \times A$, where θ is the vertical coordinate of CD spectrum, and A is the value in the absorption spectrum at the same concentration used to measure the CD spectrum.

CPL Measurements: The CPL measurements were performed on a JASCO CPL-300 spectrometer in Milli-Q water with a quartz cuvette (0.1 cm path length, Hellma) with an excitation wavelength of 400 nm. All optical measurements were performed at room temperature under ambient conditions.

Supporting Information

Supporting Information is available from the Wiley Online Library or from the author.

Acknowledgements

J.H. and F.Z. contributed equally to this work. This work was supported by the National Natural Science Foundation of Hubei Province (No. 2020CFB200), the Guangdong Basic and Applied Basic Research Foundation (2019A1515012094), and the Project of Department of Education of Guangdong Province (2018KTSCX198).

Conflict of Interest

The authors declare no conflict of interest.

Data Availability Statement

The data that support the findings of this study are available from the corresponding author upon reasonable request.

Keywords

CdSe/CdS nanoplatelets, circularly polarized luminescence, circular dichroism, island-like CdS shell, ligand-induced chirality

[1] A. Ben-Moshe, A. O. Govorov, G. Markovich, *Angew. Chem., Int. Ed.* **2013**, *52*, 1275.

[2] J. Yeom, B. Yeom, H. Chan, K. W. Smith, S. Dominguez-Medina, J. H. Bahng, G. Zhao, W.-S. Chang, S.-J. Chang, A. Chuvilin, D. Melnikau, A. L. Rogach, P. Zhang, S. Link, P. Král, N. A. Kotov, *Nat. Mater.* **2015**, *14*, 66.

[3] M. V. Mukhina, V. G. Maslov, A. V. Baranov, A. V. Fedorov, A. O. Orlova, F. Purcell-Milton, J. Govan, Y. K. Gun'ko, *Nano Lett.* **2015**, *15*, 2844.

[4] A. Kühnle, T. R. Linderoth, B. Hammer, F. Besenbacher, *Nature* **2002**, *415*, 891.

[5] A. Ben-Moshe, A. Teitelboim, D. Oron, G. Markovich, *Nano Lett.* **2016**, *16*, 7467.

[6] G. Yang, H. Zhong, *Isr. J. Chem.* **2019**, *59*, 639.

[7] S. Huo, P. Duan, T. Jiao, Q. Peng, M. Liu, *Angew. Chem., Int. Ed.* **2017**, *56*, 12174.

[8] Y. Xia, Y. Zhou, Z. Tang, *Nanoscale* **2011**, *3*, 1374.

[9] M. Sun, L. Xu, A. Qu, P. Zhao, T. Hao, W. Ma, C. Hao, X. Wen, F. M. Colombari, A. F. de Moura, N. A. Kotov, C. Xu, H. Kuang, *Nat. Chem.* **2018**, *10*, 821.

[10] E. Shah, H. P. Soni, *RSC Adv.* **2013**, *3*, 17453.

[11] L. Xiao, T. An, L. Wang, X. Xu, H. Sun, *Nano Today* **2020**, *30*, 100824.

[12] W. Ma, L. Xu, A. F. de Moura, X. Wu, H. Kuang, C. Xu, N. A. Kotov, *Chem. Rev.* **2017**, *117*, 8041.

[13] X. Zhao, S.-Q. Zang, X. Chen, *Chem. Soc. Rev.* **2020**, *49*, 2481.

[14] M. P. Moloney, Y. K. Gun'ko, J. M. Kelly, *Chem. Commun.* **2007**, *38*, 3900.

[15] S. D. Elliott, M. P. Moloney, Y. K. Gun'ko, *Nano Lett.* **2008**, *8*, 2452.

[16] Y. Zhou, M. Yang, K. Sun, Z. Tang, N. A. Kotov, *J. Am. Chem. Soc.* **2010**, *132*, 6006.

[17] T. Nakashima, Y. Kobayashi, T. Kawai, *J. Am. Chem. Soc.* **2009**, *131*, 10342.

[18] A. S. Baimuratov, I. D. Rukhlenko, Y. K. Gun'ko, A. V. Baranov, A. V. Fedorov, *Nano Lett.* **2015**, *15*, 1710.

[19] F. Purcell-Milton, A. K. Visheratina, V. A. Kuznetsova, A. Ryan, A. O. Orlova, Y. K. Gun'ko, *ACS Nano* **2017**, *11*, 9207.

[20] J. Cheng, J. Hao, H. Liu, J. Li, J. Li, X. Zhu, X. Lin, K. Wang, T. He, *ACS Nano* **2018**, *12*, 5341.

[21] G. Yang, M. Kazes, D. Oron, *Adv. Funct. Mater.* **2018**, *28*, 1802012.

[22] E. D. Sone, E. R. Zubarev, S. I. Stupp, *Angew. Chem., Int. Ed.* **2002**, *41*, 1705.

[23] Y. Zhou, R. L. Marson, G. van Anders, J. Zhu, G. Ma, P. Ercius, K. Sun, B. Yeom, S. C. Glotzer, N. A. Kotov, *ACS Nano* **2016**, *10*, 3248.

[24] W. Feng, J.-Y. Kim, X. Wang, H. A. Calcaterra, Z. Qu, L. Meshi, N. A. Kotov, *Sci. Adv.* **2017**, *3*, e1601159.

[25] U. Tohgha, K. K. Deol, A. G. Porter, S. G. Bartko, J. K. Choi, B. M. Leonard, K. Varga, J. Kubelka, G. Muller, M. Balaz, *ACS Nano* **2013**, *7*, 11094.

[26] X. Qiu, J. Hao, J. Li, Z. Gong, S. Li, J. Cheng, X. Lin, T. He, *Opt. Lett.* **2019**, *44*, 2256.

[27] Y. Shi, Z. Zhou, X. Miao, Y. J. Liu, Q. Fan, K. Wang, D. Luo, X. W. Sun, *J. Mater. Chem. C* **2020**, *8*, 1048.

[28] Y.-w. Jun, J.-s. Choi, J. Cheon, *Angew. Chem., Int. Ed.* **2006**, *45*, 3414.

[29] S. Ithurria, M. D. Tessier, B. Mahler, R. P. S. M. Lobo, B. Dubertret, A. L. Efros, *Nat. Mater.* **2011**, *10*, 936.

[30] M. D. Tessier, B. Mahler, B. Nadal, H. Heuclin, S. Pedetti, B. Dubertret, *Nano Lett.* **2013**, *13*, 3321.

[31] Y. Kelestemur, B. Guzelturk, O. Erdem, M. Olutas, K. Gungor, H. V. Demir, *Adv. Funct. Mater.* **2016**, *26*, 3570.

[32] B. Mahler, B. Nadal, C. Bouet, G. Patriarche, B. Dubertret, *J. Am. Chem. Soc.* **2012**, *134*, 18591.

[33] C. She, I. Fedin, D. S. Dolzhnikov, A. Demortière, R. D. Schaller, M. Pelton, D. V. Talapin, *Nano Lett.* **2014**, *14*, 2772.

[34] C. Ren, J. Hao, H. Chen, K. Wang, D. Wu, *Appl. Surf. Sci.* **2015**, *353*, 480.

[35] J. Hao, H. Liu, J. Miao, R. Lu, Z. Zhou, B. Zhao, B. Xie, J. Cheng, K. Wang, M.-H. Delville, *Sci. Rep.* **2019**, *9*, 12048.

[36] L. Carbone, C. Nobile, M. De Giorgi, F. D. Sala, G. Morello, P. Pompa, M. Hytch, E. Snoeck, A. Fiore, I. R. Franchini, M. Nadasan, A. F. Silvestre, L. Chiodo, S. Kudera, R. Cingolani, R. Krahne, L. Manna, *Nano Lett.* **2007**, *7*, 2942.

[37] D. V. Talapin, J. H. Nelson, E. V. Shevchenko, S. Aloni, B. Sadtler, A. P. Alivisatos, *Nano Lett.* **2007**, *7*, 2951.

[38] M. l. D. Tessier, P. Spinicelli, D. Dupont, G. Patriarche, S. Ithurria, B. Dubertret, *Nano Lett.* **2013**, *14*, 207.

[39] S. Delikanli, B. Guzelturk, P. L. Hernández-Martínez, T. Erdem, Y. Kelestemur, M. Olutas, M. Z. Akgul, H. V. Demir, *Adv. Funct. Mater.* **2015**, *25*, 4282.

[40] S. Ithurria, D. V. Talapin, *J. Am. Chem. Soc.* **2012**, *134*, 18585.

[41] X. Wang, J. Hao, J. Cheng, J. Li, J. Miao, R. Li, Y. Li, J. Li, Y. Liu, X. Zhu, Y. Liu, X. W. Sun, Z. Tang, M.-H. Delville, T. He, R. Chen, *Nanoscale* **2019**, *11*, 9327.

[42] X. Gao, X. Zhang, L. Zhao, P. Huang, B. Han, J. Lv, X. Qiu, S.-H. Wei, Z. Tang, *Nano Lett.* **2018**, *18*, 6665.

[43] B. N. Pal, Y. Ghosh, S. Brovelli, R. Laocharoensuk, V. I. Klimov, J. A. Hollingsworth, H. Htoon, *Nano Lett.* **2011**, *12*, 331.

[44] A. V. Baranov, Y. P. Rakovich, J. F. Donegan, T. S. Perova, R. A. Moore, D. V. Talapin, A. L. Rogach, Y. Masumoto, I. Nabiev, *Phys. Rev. B* **2003**, *68*, 165306.

[45] B. Ji, Y. E. Panfil, N. Waiskopf, S. Remennik, I. Popov, U. Banin, *Nat. Commun.* **2019**, *10*, 2.

[46] J. J. Li, Y. A. Wang, W. Guo, J. C. Keay, T. D. Mishima, M. B. Johnson, X. Peng, *J. Am. Chem. Soc.* **2003**, *125*, 12567.

[47] Y. Sang, J. Han, T. Zhao, P. Duan, M. Liu, *Adv. Mater.* **2019**, *32*, 1900110.

[48] W. Nan, Y. Niu, H. Qin, F. Cui, Y. Yang, R. Lai, W. Lin, X. Peng, *J. Am. Chem. Soc.* **2012**, *134*, 19685.